Experimental and numerical investigation of the reflection coefficient and the distributions of Wigner's reaction matrix for irregular graphs with absorption

Michał Ławniczak,[1] Oleh Hul,[1] Szymon Bauch,[1] Petr Seba,[2,3] and Leszek Sirko[1]
[1]*Institute of Physics, Polish Academy of Sciences, Aleja Lotników 32/46, 02-668 Warszawa, Poland*
[2]*University of Hradec Králové, Hradec Králové, Czech Republic*
[3]*Institute of Physics, Academy of Sciences of the Czech Republic, Cukrovarnická 10, 162 53 Praha, Czech Republic*
(Received 19 February 2008; published 20 May 2008)

We present the results of an experimental and numerical study of the distribution of the reflection coefficient $P(R)$ and the distributions of the imaginary $P(v)$ and the real $P(u)$ parts of the Wigner reaction K matrix for irregular fully connected hexagon networks (graphs) in the presence of strong absorption. In the experiment we used microwave networks, which were built of coaxial cables and attenuators connected by joints. In the numerical calculations experimental networks were described by quantum fully connected hexagon graphs. The presence of absorption introduced by attenuators was modeled by optical potentials. The distribution of the reflection coefficient $P(R)$ and the distributions of the reaction K matrix were obtained from measurements and numerical calculations of the scattering matrix S of the networks and graphs, respectively. We show that the experimental and numerical results are in good agreement with the exact analytic ones obtained within the framework of random matrix theory.

DOI: 10.1103/PhysRevE.77.056210 PACS number(s): 05.45.Mt, 03.65.Nk

Quantum graphs of connected one-dimensional wires were introduced more than 60 years ago by Pauling [1]. Next the same idea was used by Kuhn [2] to describe organic molecules by free electron models. Quantum graphs can be considered as idealizations of physical networks in the limit where the lengths of the wires are much bigger than their widths, i.e., assuming that the propagating waves remain in a single transversal mode. Among the systems modeled by quantum graphs one can find, e.g., electromagnetic optical waveguides [3,4], mesoscopic systems [5,6], quantum wires [7,8], and excitation of fractions in fractal structures [9,10]. Recently it has been shown that quantum graphs are excellent paradigms of quantum chaos [11–21]. More complicated and thus more realistic systems—microwave networks with moderate absorption strength $\gamma=2\pi\Gamma/\Delta\leq 7.1$, where Γ is the absorption width and Δ is the mean level spacing—have been experimentally investigated in [22,23]. Other interesting open objects—quantum graphs with leads—have been analyzed in detail in [14,15]. However, the properties of networks and graphs with strong absorption have not been studied experimentally or numerically so far. Therefore, in this paper we study experimentally and numerically the distribution of the reflection coefficient $P(R)$ and the distributions of the Wigner reaction matrix [24] (in the literature often called the K matrix [25]) for networks (graphs) with time reversal symmetry ($\beta=1$) in the presence of strong absorption.

In the case of a single-channel antenna experiment, the K matrix is related to the scattering matrix S by

$$S=\frac{1-iK}{1+iK}. \tag{1}$$

Equation (1) holds for systems with absorption but without direct processes [25]. It is important to mention that the function $Z=iK$ has the direct physical meaning of the electric impedance, which has been recently measured in a microwave cavity experiment [26]. In the one-channel case the S matrix can be parametrized as

$$S=\sqrt{R}e^{i\theta}, \tag{2}$$

where R is the reflection coefficient and θ the phase.

The properties of the statistical distributions of the S matrix with direct processes and imperfect coupling have been studied theoretically in several important papers [27–32]. Recently the distribution of the S matrix has also been measured experimentally for chaotic microwave cavities with absorption [33]. The distribution $P(R)$ of the reflection coefficient R and the distributions of the imaginary $P(v)$ and the real $P(u)$ parts of the Wigner reaction K matrix are theoretically known for any dimensionless absorption strength γ [25,34]. In the case of time-reversal systems (symmetry index $\beta=1$) $P(R)$ has been studied experimentally by Méndez-Sánchez *et al.* [35]. The distributions $P(v)$ and $P(u)$ have been studied for chaotic microwave cavities in [26,36] and for microwave networks for moderate absorption strength $\gamma\leq 7.1$ in [22,23]. For systems without time-reversal symmetry ($\beta=2$) and a single perfectly coupled channel $P(R)$ was calculated by Beenakker and Brouwer [37], while the exact formulas for the distributions $P(v)$ and $P(u)$ were given by Fyodorov and Savin [25].

In experiments, quantum graphs can be simulated by microwave networks. The analogy between quantum graphs and microwave networks is based upon the equivalency of the Schrödinger equation describing the quantum system and the telegraph equation describing the microwave circuit [21].

A general microwave network consists of N vertices connected by bonds, e.g., coaxial cables. A coaxial cable consists of an inner conductor of radius r_1 surrounded by a concentric conductor of inner radius r_2. The space between the inner and the outer conductors is filled with a homogeneous material having a dielectric constant ε. For a frequency ν below the onset of the next TE_{11} mode, only the fundamental

TEM mode can propagate inside a coaxial cable. (This mode is in the literature often called a Lecher wave.) The cutoff frequency of the TE_{11} mode is $\nu_c \simeq \frac{c}{\pi(r_1+r_2)\sqrt{\varepsilon}} = 32.9$ GHz [38], where $r_1 = 0.05$ cm is the inner wire radius of the coaxial cable (RG402), while $r_2 = 0.15$ cm is the inner radius of the surrounding conductor, and $\varepsilon \simeq 2.08$ is the Teflon dielectric constant [39,40].

From the experimental point of view, the absorption of the networks can be changed by a change of the bond (cable) lengths [21] or more effectively by the application of microwave attenuators [22,23]. In the numerical calculations weak absorption inside the cables can be described with the help of a complex wave vector [21]. We will show that strong absorption inside an attenuator can be described by a simple optical potential. The corresponding mathematical theory has been developed in [41].

The distribution $P(R)$ of the reflection coefficient R and the distributions of the imaginary and real parts of the Wigner reaction matrix K for microwave networks with absorption were found using the impedance approach [23,26,36]. In this approach the real and imaginary parts of the normalized impedance Z,

$$Z = \frac{\mathrm{Re}\, Z_n + i(\mathrm{Im}\, Z_n - \mathrm{Im}\, Z_r)}{\mathrm{Re}\, Z_r}, \tag{3}$$

of a chaotic microwave system are measured, with $Z_{n(r)} = Z_0(1+S_{n(r)})/(1-S_{n(r)})$ being the network (radiation) impedance expressed by the network (radiation) scattering matrix $S_{n(r)}$ and Z_0 the characteristic impedance of the transmission line. The radiation impedance Z_r is the impedance seen at the output of the coupling structure for the same coupling geometry, but with the vertices of the network removed to infinity. The Wigner reaction matrix K can be expressed via the normalized impedance as $K = -iZ$. The scattering matrix S of a network for the perfect coupling case (no direct processes present) required for the calculation of the reflection coefficient R [see Eq. (2)] can be finally extracted from the formula $S = (1-Z)/(1+Z)$.

Figure 1(a) shows the experimental setup for measuring the single-channel scattering matrix S_n of fully connected hexagon microwave networks necessary for finding the impedance Z_n. We used a Hewlett-Packard 8720A microwave vector network analyzer to measure the scattering matrix S_n of the networks in the frequency window: 7.5–11.5 GHz. The networks were connected to the vector network analyzer through a lead—a HP 85131-60012 flexible microwave cable—connected to a six-joint vertex. The other five vertices of the networks were connected by five joints. Each bond of the network presented in Fig. 1(a) contains a microwave attenuator.

The radiation impedance Z_r was found experimentally by measuring the scattering matrix S_r of the six-joint connector with five joints terminated by 50 Ω loads [see Fig. 1(b)].

The experimentally measured fully connected hexagon networks were described in numerical calculations by quantum fully connected hexagon graphs with one lead attached to the six-joint vertex. In the calculations, attenuators (absorbers) were modeled by optical potentials [41]. To be explicit, we suppose that the fully connected hexagon graph Υ with one coupled antenna is described in the Hilbert space $L^2(\Upsilon) := \oplus_{(j,n)} L^2(0, \ell_{jn}) \oplus L^2(0,\infty)$, where ℓ_{jn} stands for the length of the bond connecting the vertices j and n and the half line $(0,\infty)$ describes the attached antenna.

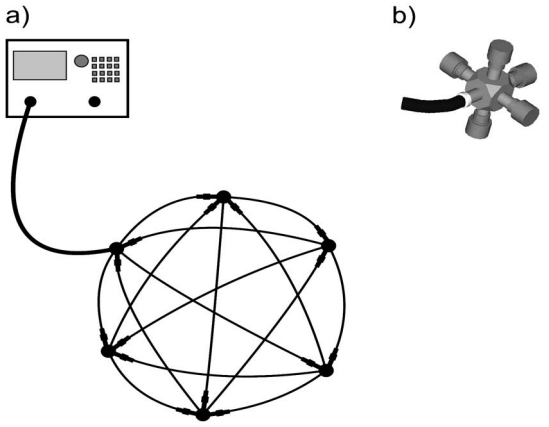

FIG. 1. (a) Scheme of the experimental setup for measurements of the scattering matrix S_n of microwave fully connected networks with absorption. Absorption in the networks was varied by change of the attenuators. (b) Scheme of the setup used to measure the radiation scattering matrix S_r. Instead of a network five 50 Ω loads were connected to the six joint.

We define the Schrödinger operator H by

$$H\psi_{jn} := -\psi''_{jn} + U_{jn}\psi_{jn} \tag{4}$$

with $\psi_{jn} \in L^2(0, \ell_{jn})$ for the bonds and

$$H\psi_{0n} := -\psi_{0n} \tag{5}$$

with $\psi_{0n} \in L^2(0,\infty)$ describing the wave function of the antenna connected to the vertex n (note that the "infinite" vertex of the antenna has index 0).

At the vertices the wave functions are linked together with the boundary values

$$\psi_{jn}(j) := \lim_{x\to 0+} \psi_{jn}(x), \quad \psi'_{jn}(j) := \lim_{x\to 0+} \psi'_{jn}(x), \tag{6}$$

satisfying the boundary conditions $\psi_{jn}(j) = \psi_{jm}(j) =: \psi_j$ for all n,m describing connected vertices, and

$$\sum_{n\in\nu(j)} \psi'_{jn}(j) = 0. \tag{7}$$

The optical potentials U_{jn} are purely imaginary and describe the absorber inserted between the vertices (j,n).

Since the graph Υ is infinite (due to the attached antenna) we can look for solutions of the equation

$$H\psi = k^2\psi, \tag{8}$$

referring to the continuous spectrum, where k is the wave vector. For microwaves propagating inside a lossless bond with a dielectric constant ε, the wave vector $k = 2\pi\varepsilon\nu/c$, where ν and c denote the frequency of a microwave field and the speed of light in the vacuum, respectively. To solve this equation we used the graph duality principle [41]. According to this principle we need to solve the equation $-f'' + U_{jn}f$

$=k^2 f$ on $[0,\ell_{jn}]$ satisfying the normalized Dirichlet boundary conditions

$$u_{jn}(\ell_{jn}) = 1 - (u_{jn})'(\ell_{jn}) = 0, \quad v_{jn}(0)1 - (v_{jn})'(0) = 0. \tag{9}$$

The Wronskian of this solution is naturally equal to $W_{jn} - v_{jn}(\ell_{jn}) = u_{jn}(0)$. Then according to [41] the corresponding boundary values (6) satisfy the equation

$$\sum_n \frac{\psi_n}{W_{jn}} - \left(\sum_{n\in\nu(j)} \frac{(v_{jn})'(\ell_{jn})}{W_{jn}} \right) \psi_j = 0. \tag{10}$$

Conversely, any solution ψ_j of the system (10) determines a solution of Eq. (8) by

$$\psi_{jn}(x) = \frac{\psi_n}{W_{jn}} u_{jn}(x) - \frac{\psi_j}{W_{jn}} v_{jn}(x) \quad \text{if } n = 1, \ldots, 6, \tag{11}$$

$$\psi_{jn}(x) = -\frac{\psi_j}{W_{jn}} v_{jn}(x) \quad \text{if } n = 0. \tag{12}$$

As already mentioned the microwave attenuators are modeled by optical potentials localized inside the inserted component. It is well known that any smooth and localized potential can be easily approximated by a sequence of δ potentials inside the support of the potential—see [42] for details. We will use this fact and express the optical potential as a sum of N δ potentials with imaginary coupling constants $U(x) = ib\Sigma_{r=1}^{N} \delta(x-(r-1)l_b/(N-1))$. The δ potentials were equally spaced inside the length l_b of the absorbing element (attenuator). By changing the number N and the strength b of the δ potentials, we were able to vary absorbing properties as well as reflective properties of the attenuators. We used $N=10$ δ potentials with $b=0.028$ m^{-1} for simulation of the 1 dB attenuators and $N=12$ δ potentials with $b=0.045$ m^{-1} for the 2 dB attenuators. In both cases the length of the attenuator was $l_b=2.65$ cm. Furthermore, in the numerical calculations of the scattering matrices S_n of the graphs, the weak absorption inside the microwave cables was taken into account by replacing the real wave vector k by the complex vector $k+ia\sqrt{k}$ [43], where the absorption coefficient was assumed to be $a=0.009$ $\mathrm{m}^{-1/2}$ [21].

In order to find the distribution $P(R)$ of the reflection coefficient R and the distributions of the imaginary and real parts of the K matrix we measured the scattering matrix S_n of 88 and 74 network configurations containing in each bond a single 1 dB and a single 2 dB microwave SMA (SubMiniature version A) attenuator, respectively. The total optical lengths of the microwave networks containing 1 dB attenuators, including joints and attenuators, varied from 574 to 656 cm. For the networks with 2 dB attenuators the optical lengths varied from 554 to 636 cm. To avoid degeneracy of eigenvalues of the networks, the lengths of the bonds were chosen as incommensurable.

In Fig. 2 the modulus $|S_n|$ and the phase θ of the scattering matrix S_n of the microwave networks with $\gamma=19.9$ and 47.9, respectively, are presented in the frequency range 7.5–9 GHz. The measurements were done for two networks containing 1 and 2 dB attenuators, respectively. Their total "optical" lengths including joints and attenuators were 574 and 554 cm, respectively.

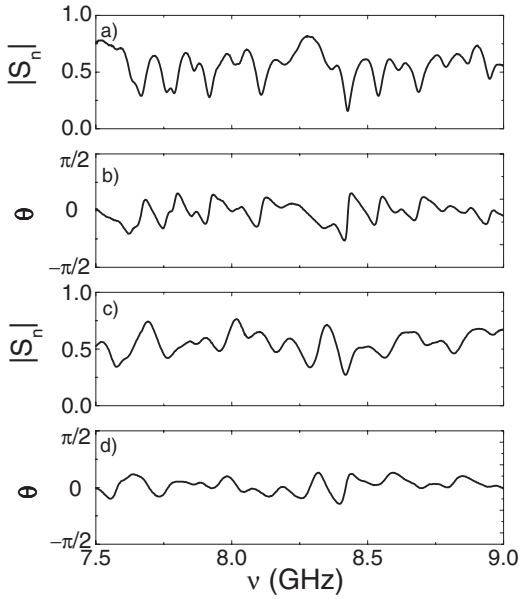

FIG. 2. (a) Modulus $|S_n|$ and (b) phase θ of the scattering matrix S measured for the network with $\gamma=19.9$ in the frequency range 7.5–9 GHz. (c) $|S_n|$ and (d) θ of the scattering matrix S_n for the network with $\gamma=47.9$ in the same frequency range. The measurements have been done for two networks which in each bond contained a 1 dB attenuator (a),(b) and a 2 dB attenuator (c),(d), respectively. The total "optical" length of the microwave networks including joints and attenuators were 574 and 554 cm, respectively.

For systems with time-reversal symmetry ($\beta=1$), the explicit analytic expression for the distribution $P(R)$ of the reflection coefficient R is given by [34]

$$P(R) = \frac{2}{(1-R)^2} P_0\left(\frac{1+R}{1-R}\right). \tag{13}$$

The probability distribution $P_0(x)$ is given by the expression

$$P_0(x) = -\frac{dW(x)}{dx}, \tag{14}$$

where the integrated probability distribution $W(x)$ is expressed by the formula [34]

$$W(x) = \frac{x+1}{4\pi}[f_1(w)g_2(w) + f_2(w)g_1(w) + h_1(w)j_2(w) + h_2(w)j_1(w)]_{w=(x-1)/2}. \tag{15}$$

The functions f_1, g_1, h_1, j_1 are defined as follows:

$$f_1(w) = \int_w^\infty dt \frac{\sqrt{t|t-w|}e^{-\gamma t/2}}{(1+t)^{3/2}} \left(1 - e^{-\gamma} + \frac{1}{t}\right), \tag{16}$$

$$g_1(w) = \int_w^\infty dt \frac{e^{-\gamma t/2}}{\sqrt{t|t-w|}(1+t)^{3/2}}, \tag{17}$$

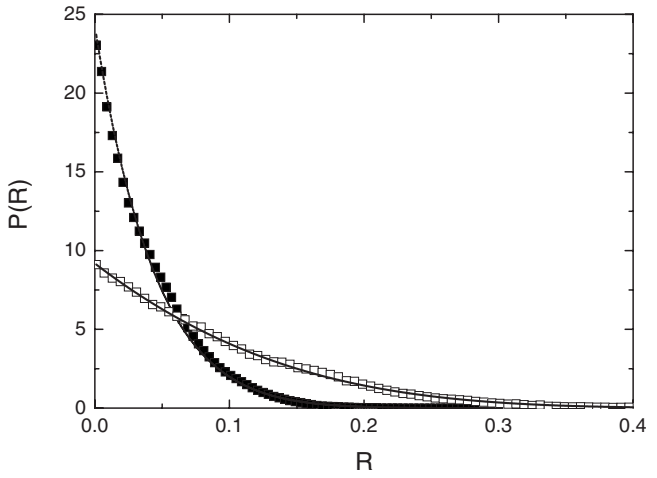

FIG. 3. Experimental distribution $P(R)$ of the reflection coefficient R for microwave fully connected hexagon networks at $\bar{\gamma}=19.3$ (open squares) and 17.7 (full squares). The corresponding theoretical distribution $P(R)$ evaluated from Eq. (13) is marked by the solid ($\gamma=19.3$) and dashed ($\gamma=47.7$) lines.

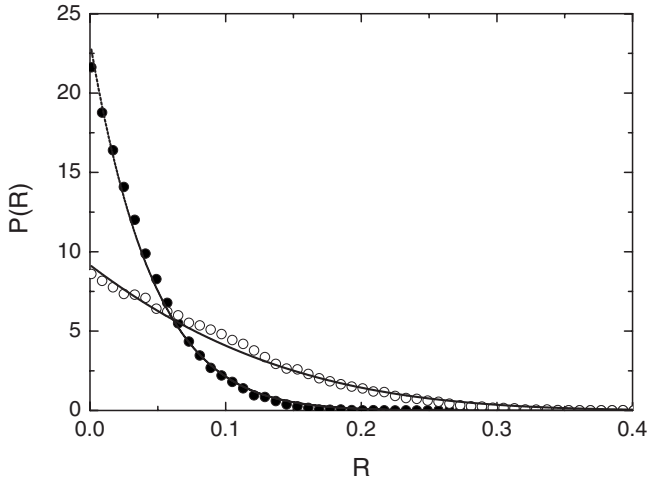

FIG. 4. Numerical distribution $P(R)$ of the reflection coefficient R for fully connected hexagon quantum graphs at $\bar{\gamma}=19.3$ (open circles) and 47.7 (full circles). The corresponding theoretical distribution $P(R)$ evaluated from Eq. (13) is marked by the solid ($\gamma=19.3$) and dashed ($\gamma=47.7$) lines.

$$h_1(w)=\int_w^\infty dt\frac{\sqrt{|t-w|}e^{-\gamma t/2}}{\sqrt{t(1+t)}}[\gamma+(1-e^{-\gamma})(\gamma t-2)], \tag{18}$$

$$j_1(w)=\int_w^\infty dt\frac{e^{-\gamma t/2}}{\sqrt{t|t-w|}(1+t)^{1/2}}. \tag{19}$$

Their counterparts with the index 2 are given by the same expressions but the integration is performed in the interval $t\in[0,w]$ instead of $[w,\infty)$.

The distributions of the imaginary and the real parts $P(v)$ and $P(u)$ of the K matrix [25] can also be expressed by the probability distribution $P_0(x)$:

$$P(v)=\frac{\sqrt{2}}{\pi v^{3/2}}\int_0^\infty dq\ P_0\left[q^2+\frac{1}{2}\left(v+\frac{1}{v}\right)\right] \tag{20}$$

and

$$P(u)=\frac{1}{2\pi\sqrt{u^2+1}}\int_0^\infty dq\ P_0\left[\frac{\sqrt{u^2+1}}{2}\left(q+\frac{1}{q}\right)\right] \tag{21}$$

where $-v=\mathrm{Im}\,K<0$ and $u=\mathrm{Re}\,K$ are, respectively, the imaginary and real parts of the K matrix.

Figure 3 shows the experimental distributions $P(R)$ (squares) of the reflection coefficient R for two mean values of the parameter $\bar{\gamma}$, viz., 19.3 and 47.7. The distribution for $\bar{\gamma}=19.3$ is obtained by averaging over 88 realizations of the microwave networks containing 1 dB attenuators. The distribution for $\bar{\gamma}=47.7$ is obtained by averaging over 74 realizations of the microwave networks containing 2 dB attenuators. The experimental values of the γ parameter were estimated for each realization of the network by adjusting the theoretical mean reflection coefficient $\langle R\rangle_{th}$ to the experimental one $\langle R\rangle=\langle SS^\dagger\rangle$, where

$$\langle R\rangle_{th}=\int_0^1 dR\ RP(R). \tag{22}$$

Figure 3 also presents the corresponding distributions $P(R)$ (solid and dashed lines, respectively) evaluated from Eq. (13). A good overall agreement of the experimental distributions $P(R)$ with their theoretical counterparts is seen.

Figure 4 shows the numerically evaluated distributions $P(R)$ (circles) of the reflection coefficient R for the graphs at $\bar{\gamma}=19.3$ and 47.7 compared to the theoretical ones evaluated from the formula Eq. (13). The numerical distributions are the result of averaging over 162 and 214 realizations of the graphs with optical potentials simulating 1 and 2 dB attenuators, respectively. The numerical values of the γ parameter were also estimated by adjusting the theoretical mean reflection coefficient to the numerical one. The agreement between the numerical results for $\bar{\gamma}=47.7$ and the theoretical ones (dashed line) is good. However, for $\bar{\gamma}=19.3$ for $R<0.15$ some discrepancies between the numerical results and the theoretical ones (solid line) are visible.

In Fig. 5 the experimental distribution $P(v)$ of the imaginary part of the K matrix is shown for the two mean values of the parameter $\bar{\gamma}=19.3$ and 47.7, respectively. The distribution is the result of averaging over 88 and 74 realizations of the networks with the attenuators 1 and 2 dB, respectively. The experimental results in Fig. 5 are in general in good agreement with the theoretical ones. However, both experimental distributions are slightly higher than the theoretical ones in the vicinity of their maxima.

Results of the numerical calculations of the distributions $P(v)$ are shown in Fig. 6 for two mean values of the parameter $\bar{\gamma}=19.3$ and 47.7, respectively. They are compared to the theoretical ones evaluated from the formula Eq. (20). Figure 6 shows also a good agreement between the numerical and theoretical results, which confirms usefulness of the optical potential approach in describing the microwave attenuators.

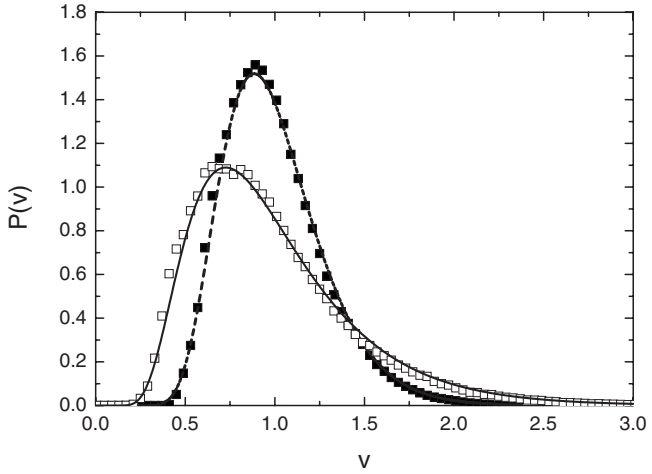

FIG. 5. Experimental distribution $P(v)$ of the imaginary part of the K matrix for the two values of the mean absorption parameter: $\bar{\gamma}=19.3$ (open squares) and 47.7 (full squares). The corresponding theoretical distribution $P(v)$ evaluated from Eq. (20) is marked by the solid ($\gamma=19.3$) and dashed ($\gamma=47.7$) lines.

Measurements of the distribution $P(u)$ of the real part of the Wigner's reaction matrix give an additional test of the consistency of the γ evaluation. In Fig. 7 we show this distribution obtained for two values of $\bar{\gamma}=19.3$ and 47.7, respectively, compared to the theoretical ones evaluated from the formula Eq. (21). Also here we observe good overall agreement between the experimental and theoretical results. However, Fig. 7 shows that for the networks with 2 dB attenuators the theoretical distribution is in the middle ($-0.1 < u < 0.1$) slightly higher than the experimental one. According to the definition of the K matrix [see Eq. (1)] such a behavior of the experimental distribution $P(u)$ suggests a deficiency of small values of $|\mathrm{Im}\, S|$, whose origin is not known. Moreover, the experimental distribution $P(u)$ obtained for the networks assembled with 1 dB attenuators is slightly asymmetric for $|u|>0.5$.

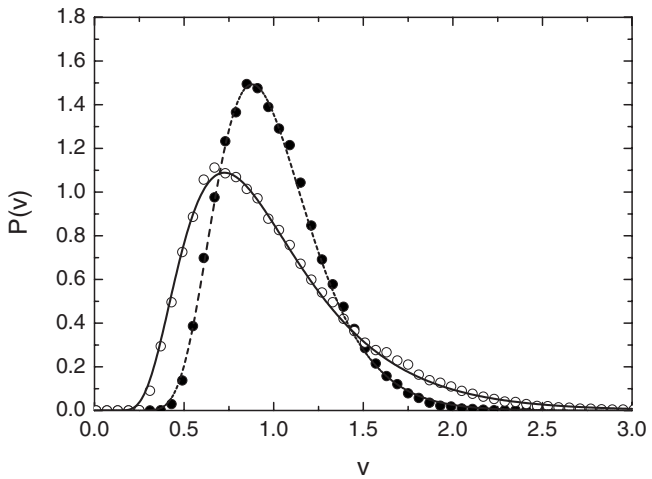

FIG. 6. Numerical distribution $P(v)$ of the imaginary part of the K matrix for the two values of the mean absorption parameter $\bar{\gamma}=19.3$ (open circles) and 47.7 (full circles). The corresponding theoretical distribution $P(v)$ evaluated from Eq. (20) is marked by the solid ($\gamma=19.3$) and dashed ($\gamma=47.7$) lines.

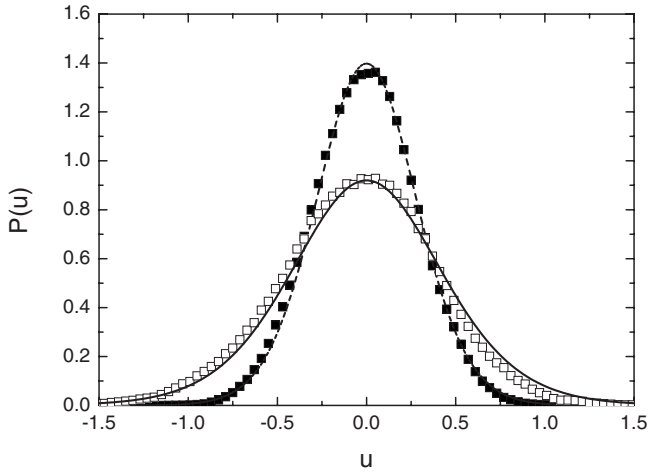

FIG. 7. Experimental distribution $P(u)$ of the real part of the K matrix for the two values of the mean absorption parameter $\bar{\gamma}=19.3$ (open squares) and 47.7 (full squares). The experiment is compared to the theoretical distribution $P(u)$ evaluated from Eq. (21): solid line ($\gamma=19.3$) and dashed line ($\gamma=47.7$).

In Fig. 8 the comparison of the numerical distribution $P(u)$ obtained for two values of $\bar{\gamma}=19.3$ and 47.7, respectively, to the theoretical one evaluated from the formula Eq. (21) is presented. In this case we see a good overall agreement between the numerical and theoretical results.

In spite of the above mentioned discrepancies, which appeared mainly in the case of the experimental distribution $P(u)$, the overall good agreement between the experimental and theoretical results justifies *a posteriori* the chosen procedure for calculating the experimental γ. The same is true also for the numerical simulations.

In summary, we measured and calculated numerically the distribution of the reflection coefficient $P(R)$ and the distributions of the imaginary $P(v)$ and the real $P(u)$ parts of the Wigner reaction K matrix for irregular fully connected hexa-

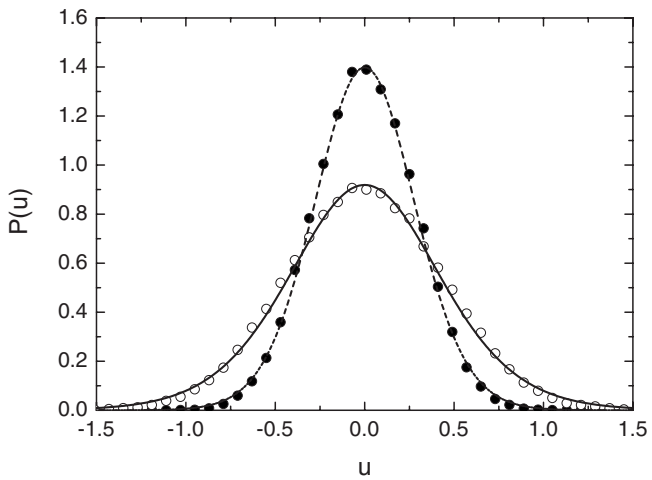

FIG. 8. Numerical distribution $P(u)$ of the real part of the K matrix for two values of the mean absorption parameter: $\bar{\gamma}=19.3$ (open circles) and 47.7 (full circles). The numerical results are compared to the theoretical distributions $P(u)$ evaluated from Eq. (21): solid line ($\gamma=19.3$) and dashed line ($\gamma=47.7$).

gon networks and graphs in the presence of strong absorption. In the case of microwave networks consisting of cables and attenuators, the application of attenuators allowed for effective change of absorption in the graphs. In the numerical calculations absorption in an attenuator was modeled by an optical potential. We showed that in the case of time-reversal symmetry ($\beta=1$), the experimental and numerical results for $P(R)$, $P(v)$, and $P(u)$ are in good overall agreement with the theoretical predictions. The agreement of the numerical and theoretical results strongly confirms the usefulness of the optical potential approach in the description of microwave attenuators.

This work was partially supported by Polish Ministry of Science and Higher Education Grant No. N202 099 31/0746 and by the Ministry of Education, Youth and Sports of the Czech Republic within Project No. LC06002.

[1] L. Pauling, J. Chem. Phys. **4**, 673 (1936).
[2] H. Kuhn, Helv. Chim. Acta **31**, 1441 (1948).
[3] C. Flesia, R. Johnston, and H. Kunz, Europhys. Lett. **3**, 497 (1987).
[4] R. Mitra and S. W. Lee, *Analytical Techniques in the Theory of Guided Waves* (Macmillan, New York, 1971).
[5] Y. Imry, *Introduction to Mesoscopic Systems* (Oxford University Press, New York, 1996).
[6] D. Kowal, U. Sivan, O. Entin-Wohlman, and Y. Imry, Phys. Rev. B **42**, 9009 (1990).
[7] E. L. Ivchenko and A. A. Kiselev, JETP Lett. **67**, 43 (1998).
[8] J. A. Sanchez-Gil, V. Freilikher, I. Yurkevich, and A. A. Maradudin, Phys. Rev. Lett. **80**, 948 (1998).
[9] Y. Avishai and J. M. Luck, Phys. Rev. B **45**, 1074 (1992).
[10] T. Nakayama, K. Yakubo, and R. L. Orbach, Rev. Mod. Phys. **66**, 381 (1994).
[11] T. Kottos and U. Smilansky, Phys. Rev. Lett. **79**, 4794 (1997).
[12] T. Kottos and U. Smilansky, Ann. Phys. (N.Y.) **274**, 76 (1999).
[13] T. Kottos and U. Smilansky, Phys. Rev. Lett. **85**, 968 (2000).
[14] T. Kottos and H. Schanz, Physica E (Amsterdam) **9**, 523 (2001).
[15] T. Kottos and U. Smilansky, J. Phys. A **36**, 3501 (2003).
[16] F. Barra and P. Gaspard, J. Stat. Phys. **101**, 283 (2000).
[17] G. Tanner, J. Phys. A **33**, 3567 (2000).
[18] P. Pakoński, K. Życzkowski, and M. Kuś, J. Phys. A **34**, 9303 (2001).
[19] P. Pakoński, G. Tanner, and K. Życzkowski, J. Stat. Phys. **111**, 1331 (2003).
[20] R. Blümel, Y. U. Dabaghian, and R. V. Jensen, Phys. Rev. Lett. **88**, 044101 (2002).
[21] O. Hul, S. Bauch, P. Pakoński, N. Savytskyy, K. Życzkowski, and L. Sirko, Phys. Rev. E **69**, 056205 (2004).
[22] O. Hul and O. Tymoshchuk, Sz. Bauch, P. M. Koch and L. Sirko, J. Phys. A **38**, 10489 (2005).
[23] O. Hul, S. Bauch, M. Ławniczak, and L. Sirko, Acta Phys. Pol. A **112**, 655 (2007).
[24] G. Akguc and L. E. Reichl, Phys. Rev. E **64**, 056221 (2001).
[25] Y. V. Fyodorov and D. V. Savin, JETP Lett. **80**, 725 (2004).
[26] S. Hemmady, X. Zheng, E. Ott, T. M. Antonsen, and S. M. Anlage, Phys. Rev. Lett. **94**, 014102 (2005).
[27] G. López, P.A. Mello, and T.H. Seligman, Z. Phys. A **302**, 351 (1981).
[28] E. Doron and U. Smilansky, Nucl. Phys. A. **545**, 455 (1992).
[29] P. W. Brouwer, Phys. Rev. B **51**, 16878 (1995).
[30] D. V. Savin, Y. V. Fyodorov, and H.-J. Sommers, Phys. Rev. E **63**, 035202(R) (2001).
[31] Y. V. Fyodorov, JETP Lett. **78**, 250 (2003).
[32] Y. V. Fyodorov, D. V. Savin, and H.-J. Sommers, J. Phys. A **38**, 10731 (2005).
[33] U. Kuhl, M. Martinez-Mares, R. A. Méndez-Sánchez, and H.-J. Stöckmann, Phys. Rev. Lett. **94**, 144101 (2005).
[34] D. V. Savin, H.-J. Sommers, and Y. V. Fyodorov, JETP Lett. **82**, 544 (2005).
[35] R. A. Méndez-Sánchez, U. Kuhl, M. Barth, C. H. Lewenkopf, and H.-J. Stöckmann, Phys. Rev. Lett. **91**, 174102 (2003).
[36] S. Hemmady, X. Zheng, T. M. Antonsen, Jr., E. Ott, and S. M. Anlage, Acta Phys. Pol. A **109**, 65 (2006).
[37] C. W. J. Beenakker and P. W. Brouwer, Physica E (Amsterdam) **9**, 463 (2001).
[38] D. S. Jones, *Theory of Electromagnetism* (Pergamon, Oxford, 1964), p. 254.
[39] K. H. Breeden and A. P. Sheppard, Microwave J. **10**, 59 (1967); Radio Sci. **3**, 205 (1968).
[40] N. Savytskyy, A. Kohler, S. Bauch, R. Blümel, and L. Sirko, Phys. Rev. E **64**, 036211 (2001).
[41] P. Exner, Ann. Inst. Henri Poincare, Sect. A **66**, 359 (1997).
[42] Y. N. Demkov and V. N. Ostrovskij, *Method of Zero-Range Potentials in Atomic Physics* (Leningrad University Press, Leningrad, 1975) (in Russian).
[43] G. Goubau, *Electromagnetic Waveguides and Cavities* (Pergamon, Oxford, 1961).